

*Article*

## **Application of Porous Nickel-Coated TiO<sub>2</sub> for the Photocatalytic Degradation of Aqueous Quinoline in an Internal Airlift Loop Reactor**

Suiyi Zhu, Xia Yang \*, Wu Yang, Leilei Zhang, Jian Wang and Mingxin Huo \*

Department of Environmental Science and Engineering, Northeast Normal University, Changchun 130024, China; E-Mails: zhuisuiyi@163.com (S.Z.); kaimomicrobial@126.com (W.Y.); zhangll@126.com (L.Z.); wangj@126.com (J.W.)

\* Authors to whom correspondence should be addressed; E-Mails: nanomatre@126.com (X.Y.); papermanuscript@126.com (M.H.); Tel.: +86-0431-8509-9169; Fax: +86-0431-8509-9169.

*Received: 31 December 2011; in revised form: 2 February 2012 / Accepted: 9 February 2012 / Published: 15 February 2012*

---

**Abstract:** P25 film, prepared by a facile dip-coating method without any binder, was further developed in a recirculating reactor for quinoline removal from synthetic wastewater. Macroporous foam Ni, which has an open three-dimensional network structure, was utilized as a substrate to make good use of UV rays. Field emission scanning electron microscopy and X-ray diffraction analysis showed that the coated/calcinated P25 films consisted of two crystal phases, and had a number of uniform microcracks on the surface. The effects of initial quinoline concentration, light intensity, reaction temperature, aeration, and initial pH were studied. Increased reaction time, light intensity, environmental temperature, and gas aeration were found to significantly improve the quinoline removal efficiency. The aeration effect of oxygen dependency on the quinoline degradation had the trend pure oxygen > air > no gas > pure nitrogen with free O<sub>2</sub>. The solution pH crucially affected quinoline photodegradation; the high electrostatic adsorption of quinoline molecules on the TiO<sub>2</sub> surface was strongly pH dependent. 2-Pyridine-carboxaldehyde, 3-pyridinecarboxaldehyde, and 2(1*H*)-quinolinone were identified as the major intermediates of quinoline degradation. Based on these intermediates, a primary degradation mechanism was proposed. This reusable P25 film benefits the photodegradation of water contaminants and has potential in other various applications.

**Keywords:** quinoline; photocatalysis; porous nickel; aeration; water purification

---

## 1. Introduction

Quinoline, a representative heterocyclic nitrogen (N) compound, is widely used as a raw material in different industries (e.g., petroleum, chemical, medical, and pesticide). Due to the presence of N in this heterocyclic compound, quinoline has a low Henry constant and high water solubility. Hence, quinoline is difficultly biodegradable, tends to accumulate in natural water environments [1], and has toxic properties. Consequently, quinoline is gaining attention given the health risks it poses [2].

The use of TiO<sub>2</sub> is an attractive technique for the complete destruction of undesirable liquid and gaseous contaminants by ultraviolet (UV) light or solar illumination. For quinoline degradation, many microscale/nanoscale catalysts like phase-pure TiO<sub>2</sub>, TiO<sub>2</sub> (Degussa P25), doped TiO<sub>2</sub>, and WO<sub>3</sub> [3-6] have been applied in different slurry systems. For example, the use of S-doped TiO<sub>2</sub> powder in a stirred slurry reactor presented high degradation efficiency under these experimental conditions regardless of the catalyst recovery and reuse [5,6], whereas both OH· and O<sub>2</sub>· radicals generated in the photocatalytic process led to the opening of a heterocyclic ring [7]. Some cases mainly focused on suspended slurry systems and proved that nanometer TiO<sub>2</sub> powders with high crystallinities and large specific surface areas are efficient for water purification at ambient conditions.

However, photocatalyst separation from a suspension and the aggregation of dispersed particles in a slurry reactor hamper the practical applications of TiO<sub>2</sub> powders [8]. Hence, recent studies have focused on the development of nano-TiO<sub>2</sub> immobilized on different substrates to increase the photocatalytic degradation efficiency as well as avoid the abovementioned separation and aggregation limitations. TiO<sub>2</sub> coated/calculated on a porous substrate has also been experimentally found to enhance the photocatalytic efficiency of TiO<sub>2</sub> films by enlarging the Brunauer-Emmett-Teller (BET) surface area and TiO<sub>2</sub> loaded amount [9,10]. A few researchers have reported a nano-TiO<sub>2</sub>-coated porous metal for the photocatalytic degradation of indoor volatile organic compounds [11]. However, to our knowledge, studies on the design and use of a photocatalytic reactor based on a TiO<sub>2</sub> film-coated nickel (Ni) foam for the degradation of aqueous pollutants is very limited. Such studies have very significant implications in the treatment of industrial wastewater.

The present study aimed to investigate the applicability of a Degussa P25 TiO<sub>2</sub> film coated/calculated on porous Ni in a new tubular photocatalytic reactor for the minimization of model wastewater containing quinoline. The influence of various parameters (*i.e.*, initial concentration, environmental temperature, light intensity, aeration, and pH) on the efficiency of the process was assessed to optimize the degradation. The photocatalytic stability of the P25 film was also evaluated.

## 2. Materials and Methods

### 2.1. Materials

Quinoline (C<sub>9</sub>H<sub>7</sub>N, MW = 129) was acquired from Sinopharm, China, and used without further purification. TiO<sub>2</sub> (P25; ca. 80% anatase and 20% rutile) was purchased from Degussa, Germany, and

had a BET surface area of 55 m<sup>2</sup>/g. Anhydrous alcohol was obtained from Sigma. The natural pH of the synthetic wastewater containing quinoline was 6.7. Prior to photodegradation, the pH of the wastewater was adjusted using a small amount of either H<sub>2</sub>SO<sub>4</sub> or NaOH, and was monitored by a digital pH meter (WTW Multi 340i, Germany). All chemicals used were reagent grade. The distilled water used to prepare all sample solutions was prepared in our laboratory.

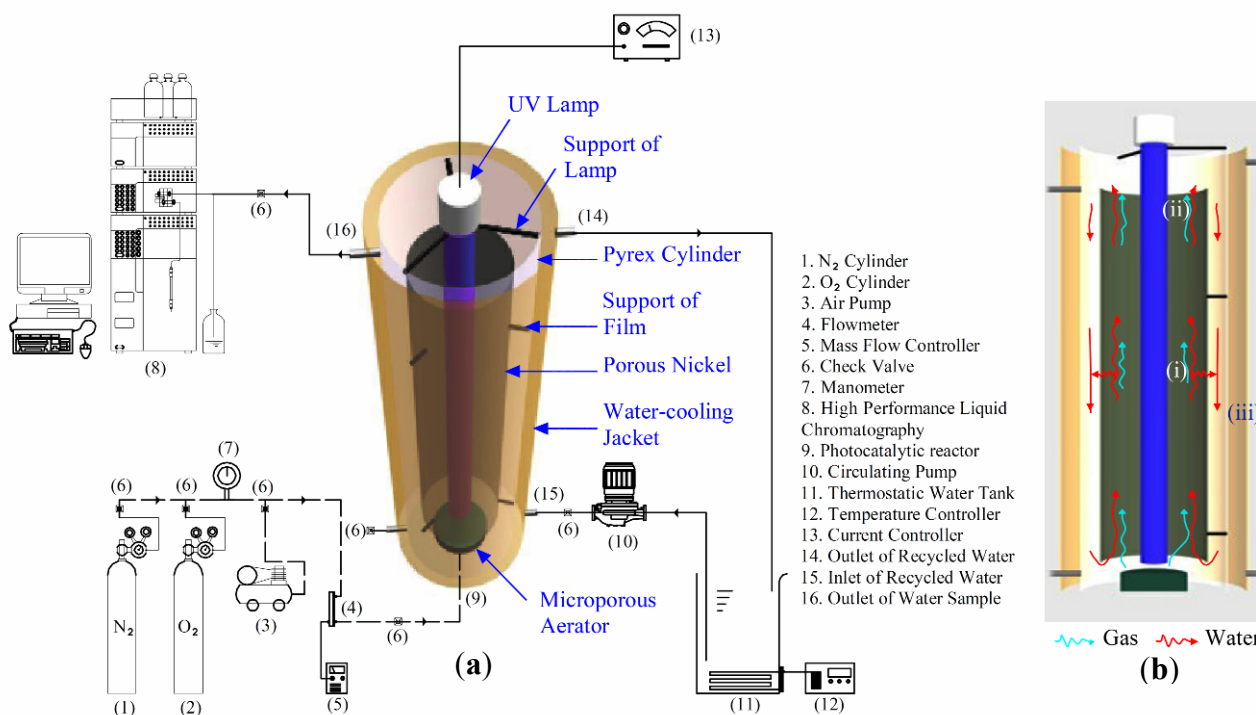
## 2.2. Preparation and Characterization of the Photocatalyst

Degussa P25 TiO<sub>2</sub> was immobilized on porous Ni (denoted as TiO<sub>2</sub>/Ni) via a facile dip-coating method without the use of coating equipment, as reported in our previous study [12]. P25 TiO<sub>2</sub> was added to anhydrous alcohol [13], and then dispersed for 10 min under ultrasonic agitation to confer the P25 sol to 10% concentration.

Foam Ni with a specific surface area of 0.25 m<sup>2</sup>/g was used as a support because of its homogeneous vesicular structure and facile machining properties, which are beneficial to increasing the contact of photocatalysts with UV rays [14,15]. Pre-dried foam Ni was cut into tubes of 40 cm × Ø 7 cm, and then immersed into the P25 sol for 20 s. The tubes were taken out and air dried at room temperature. After ethanol volatilization overnight, the TiO<sub>2</sub>/Ni film was calcined at 90 °C for 60 min, and then at 450 °C for 30 min at a heating rate of 3 °C/min in a muffle furnace. The TiO<sub>2</sub>/Ni film obtained was washed with boiling water to remove uncoated TiO<sub>2</sub> particles. The surface morphology of the prepared TiO<sub>2</sub>/Ni film and bare porous Ni substrate were observed using a field emission scanning electron microscopy (FESEM) system (XL-30 ESEM FEG, Philips). The crystal phase structures were measured by X-ray diffraction (XRD) on a Rigaku D/max-3c diffractometer (CuKα radiation, λ = 0.15405 nm). The specific surface area of the prepared TiO<sub>2</sub>/Ni film was 8.5 m<sup>2</sup>/g, as determined by nitrogen adsorption-desorption measurements (TriStar 3000).

## 2.3. Photocatalytic Reactor

An internal airlift loop photocatalytic reactor made of Pyrex glass was used for the photocatalytic experiments, as shown in Figure 1. The effective volume of the reactor was 3.5 L, and the dimensions were 55 cm × Ø 10 cm. A UV lamp (15 W, 254 nm) was longitudinally fixed in the center of the reactor. The prepared tubular TiO<sub>2</sub>/Ni film was placed on a fixed support outside the UV lamp, resulting in a 2.5 cm gap. A microporous aerator was fixed below the reactor to maintain aerobic conditions inside the TiO<sub>2</sub>/Ni tube. Gas bubbled up from the bottom and accelerated around the liquid. The liquid inside the TiO<sub>2</sub>/Ni tube flowed in two directions: (i) some liquid gradually flowed out through the tube pores, and (ii) the others flowed up to the top of the tube. Consequently, the liquid outside the tube flowed down from the top; (iii) due to the different internal and external flow rates, resulting in water circulation in the photocatalytic reactor. This process benefited the enhancement of the contacting probability between the water contaminant and the P25 TiO<sub>2</sub> on the surface of porous Ni. The experimental temperature of the entire photoreactor was controlled by a surrounding external water-cooling jacket.

**Figure 1.** Schematic diagram (a) and cross section (b) of the tubular photocatalytic reactor.

#### 2.4. Procedure and Analysis

In the photocatalytic process, 3.5 L of aqueous quinoline solution was poured into the reactor. The UV lamp was switched on to start the photo-oxidation process. Compressed gas was bubbled upward through the gas distributor at the bottom of the reactor. At pre-defined irradiation times, 50  $\mu$ L of solution was collected and immediately analyzed to avoid further reaction. The dependences of the quinoline degradation rate on initial concentration, light intensity, reaction temperature, aeration, and pH were investigated. Each experiment was conducted three times under identical conditions. The data presented in the text and figures are the mean values. The light absorption characteristics of the solutions were recorded using Persee T6 UV/visible spectrophotometer at a distance of 100 cm from the light source per the manufacturer's instructions [16]. The concentration of quinoline was analyzed using a high-performance liquid chromatography system (LC-20A). The chromatographic column was a Shim-pack VP-ODS-C18 (4.6 mm  $\times$  150 mm, 5  $\mu$ m). The mobile phase was a mixture of methanol and water (60:40, v/v) with a flow rate of 1 mL/min. The testing wavelength was 275 nm.

To obtain the intermediate products of quinoline degradation, the experiment was performed in a photocatalytic reactor with 100 mg/L quinoline under ambient conditions. After 30 min of irradiation time, 200 mL of the effluent was collected in a separating funnel, and then extracted for qualitative analysis by gas chromatography (GC)/mass spectroscopy (MS). The effluent for the GC/MS sample was further assayed by the method of Li *et al.* [17], except that 30 mL of anhydrous ether was used as the extractant. The extracts were decanted into a rotary evaporator, and then dried at 35  $^{\circ}$ C to evaporate the ether. The residue was dissolved in 10 mL of anhydrous ether for the GC/MS analysis.

GC/MS analysis was performed on an Agilent GC system (6890N/MSD 5973) equipped with an HP-5MS fused silica capillary column (30 m  $\times$  0.25 mm i.d., 0.25  $\mu$ m film thickness). The column was

first heated to 80 °C, kept constant for 3 min, linearly programmed to increase to a final temperature of 300 °C at a rate of 10 °C/min, and then isothermally held for 2 min. The temperature for the MS ion source was 200 °C, and the electron energy was 70 eV.

### 3. Results and Discussion

#### 3.1. TiO<sub>2</sub>/Ni Film Characterizations

The FESEM images of porous Ni and the TiO<sub>2</sub>/Ni film are shown in Figure 2. The surface of bare porous Ni without immobilized P25 was smooth (Figure 2a). After P25 TiO<sub>2</sub> coating, the originally smooth surface of the coated TiO<sub>2</sub>/Ni film (Figure 2b) became relatively rough and had a number of microcracks. Then, the specific surface area increased remarkably from 0.25 m<sup>2</sup>/g to 8.5 m<sup>2</sup>/g. Consequently, a high photocatalytic efficiency was obtained because there were more interfaces between the catalyst and reactants.

**Figure 2.** FESEM images of porous nickel substrate (a) and the TiO<sub>2</sub>/Ni film (b).

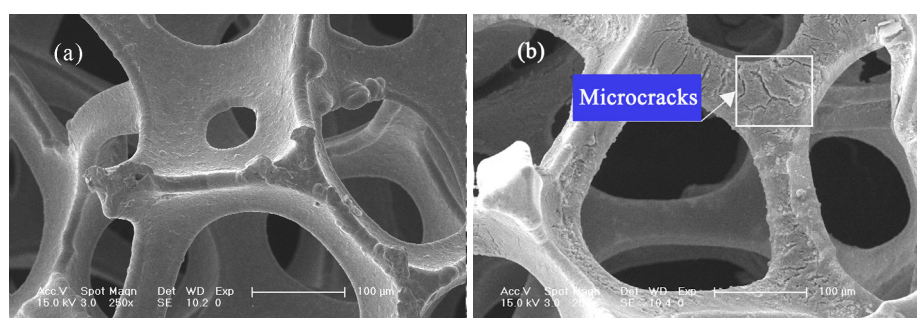
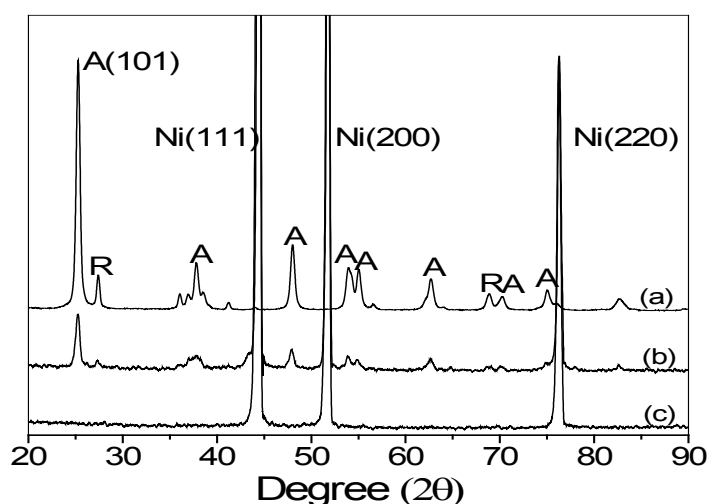


Figure 3 shows the XRD patterns of P25 TiO<sub>2</sub> powder, TiO<sub>2</sub>/Ni film, and porous Ni. Three strong diffraction peaks found at  $2\theta = 44.5^\circ$ ,  $51.8^\circ$ , and  $76.1^\circ$  were ascribed to the (111), (200), and (220) planes of Ni (ICDD PDF Card 87-0712) (JCPDS, 2001), respectively, in accordance with earlier studies [18,19].

**Figure 3.** XRD pattern of Degussa P25 TiO<sub>2</sub> (a), the TiO<sub>2</sub>/Ni film (b) and the bare nickel substrate (c). A and R denotes the anatase and rutile crystal phases, respectively.

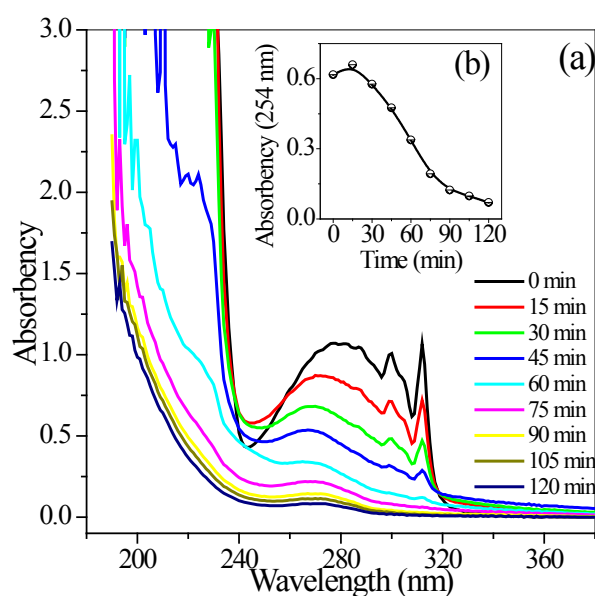


Two diffraction peaks at  $2\theta = 37.2^\circ$  and  $68.3^\circ$  were attributed to rutile phase (ICDD PDF Card 21-1276) [20]. The presence of other crystallographic plains labeled with “A” belongs to the anatase phase (ICDD PDF Card 21-1272) [20]. P25  $\text{TiO}_2$  coated on porous Ni caused no apparent change in the half width of the anatase (101) XRD peak, regardless of the heating treatment, and the crystallite size was calculated to be 21 nm from the anatase (101) peak width using the Scherrer equation. This result indicated that nano-sized  $\text{TiO}_2$  particles in P25 sol have been reproduced onto the surface of porous Ni. Therefore, the  $\text{TiO}_2/\text{Ni}$  film possessed good photocatalytic activity.

### 3.2. Photodegradation of Quinoline in the Photocatalytic Reactor

To analyze the degradation process of quinoline, a UV absorption experiment was performed on the reactants, as described in the Materials and Methods Section. With increased illumination time, a series of UV absorption spectra was recorded within the 180–380 nm range, as shown in Figure 4a. The characteristic absorption of quinoline significantly decreased with increased irradiation time, and almost disappeared at 60 min. The  $\text{UV}_{254}$  of the reaction solution initially increased and then gradually decreased. The peak appeared at 15 min (Figure 4b). This finding indicated that the aromatic or pyridine ring of quinoline opened in the initial stage, and formed a series of intermediate products containing conjugated double bond. As a result,  $\text{UV}_{254}$  absorbance was enhanced. UV absorbance within the range 180–240 nm also gradually decreased with prolonged irradiation time. This result indicated the further mineralization of aliphatic saturated as well as cyclic hydrocarbons and their derivatives in solution [21]. Interestingly, UV absorbance above 320 nm initially increased, reached the peak at 45 min, and then apparently decreased. These findings were in accordance with the color of the reaction solution changing from transparent to pale yellow, to yellow-green, and then back to transparent.

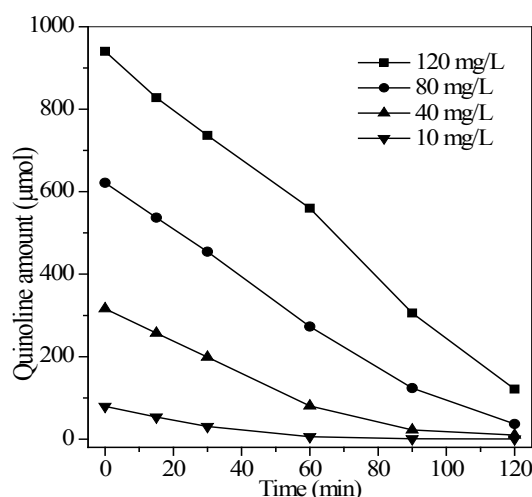
**Figure 4.** Absorbance curves (a) and  $\text{UV}_{254}$  (b) of aqueous quinoline solution. Conditions:  $C_0 = 40 \text{ mg/L}$ ,  $T = 290 \text{ K}$ , flow rate =  $0.35 \text{ L/min}$ , pH = 6.7, and the maximum irradiation intensity.



### 3.2.1. Effect of the Initial Quinoline Concentration

The effect of the initial quinoline concentration on the degradation efficiency was investigated within the range 10–120 mg/L, as shown in Figure 5. An initial aqueous quinoline concentration of 10 mg/L can almost be completely removed after 60 min of irradiation. Increased quinoline concentrations from 10 mg/L to 120 mg/L resulted in the increase in irradiation time. Moreover, the total removal amount of quinoline also increased from 78.74  $\mu\text{mol}$  to 818.78  $\mu\text{mol}$ . This result suggested that increased initial concentration obviously decreased the degradation ratio, but resulted in a high total removal amount of quinoline. Generally, the formation of activated radicals (e.g., OH and  $\text{O}_2^-$ ) on the  $\text{TiO}_2$  surface remains constant for a given light intensity, catalyst amount, air flow, and duration of irradiation. A higher quinoline concentration corresponded to a higher demand for activated radicals, resulting in prolonged reaction time for the complete decomposition. However, high initial concentrations may prompt the contact between the active radicals and quinoline molecules, thereby improving the total amount of quinoline removed.

**Figure 5.** Effect of the initial quinoline concentration on the photocatalytic degradation. Conditions:  $T = 290$  K, flow rate = 0.35 L/min, pH = 6.7, and the maximum irradiation intensity.

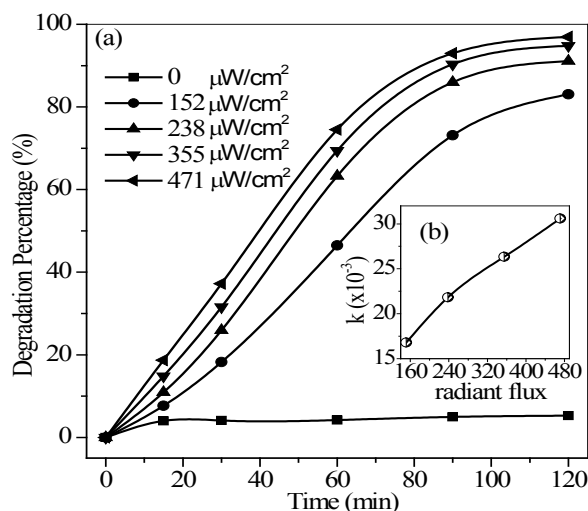


### 3.2.2. Effect of Light Intensity

A control signal processed by a digital PID regulator was used to control the input current and change the UV light output intensity. Figure 6a shows that under dark conditions, only about 5% of the quinoline was removed from synthetic water during the first 15 min, and remained constant for nearly 100 min regardless of air flow. This finding suggested that the main removal effect in the absence of UV irradiation is due to the adsorption on the  $\text{TiO}_2$  surface [22]. Interestingly, the oxidation and air stripping controlled by the gas aeration had little effect on quinoline photodegradation. However, UV irradiation benefited the removal efficiency of quinoline in water, and the degradation percent reached over 80% after 120 min of reaction at  $152 \mu\text{w}/\text{cm}^2$  of light intensity. Increased light intensity also resulted in increased photodegradation efficiency. This finding may be due to the fact that the rate of electron-hole pair formation at the  $\text{TiO}_2$  surface increased with increased light intensity to improve the photocatalytic efficiency. Figure 6b shows an acceptably good linear correlation between the apparent

first-order rate constant and light intensity. This tendency indicated that light intensity is an important control agent of photocatalytic reaction within the radiant flux range of 152 to 471  $\mu\text{W}/\text{cm}^2$ .

**Figure 6.** Degradation percentage (a) and reaction rate (b) with respect to different radiant flux. Conditions:  $T = 290\text{ K}$ , flow rate = 0.35 L/min, pH = 6.7, and  $C_0 = 40\text{ mg/L}$ .

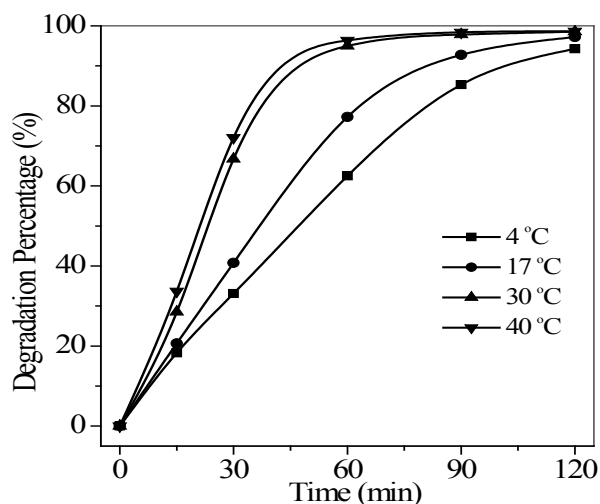


### 3.2.3. Effect of Reaction Temperature

The dependence of the quinoline degradation rate on the reaction temperature within 4–40  $^{\circ}\text{C}$  was also determined. Figure 7 shows that compared with the degradation percent at 60 min, the degradation ratio rapidly increased within 4–30  $^{\circ}\text{C}$ , and then very gradually increased above 30  $^{\circ}\text{C}$ .

Warm temperatures enhance the collision frequency of molecules [23]. Hence, the movement of the reactant molecules continued to intensify and gradually reached a plateau. However, for  $\text{TiO}_2$  photocatalysis, electron-hole pair generation at ambient temperatures is mainly affected by light irradiation given that the band gap energy is too high to be overcome by thermal activation [24]. Therefore, the increase in percent quinoline degradation was most likely due to the enhanced collision frequency with the increased reaction temperature.

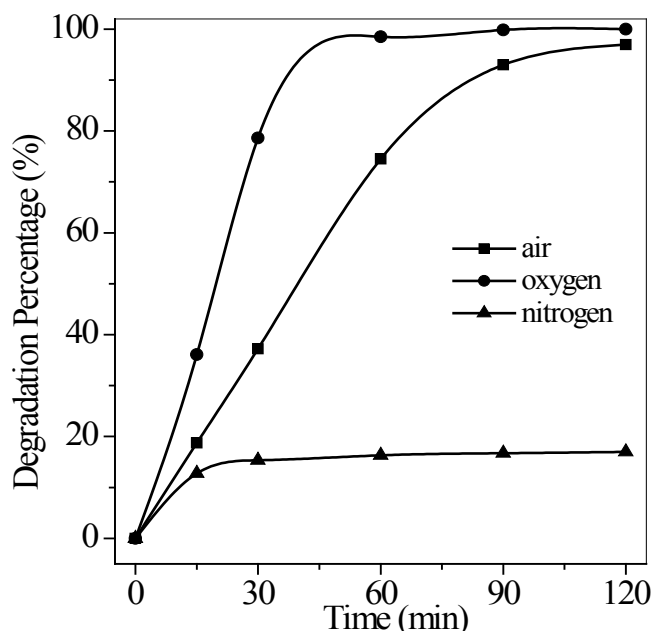
**Figure 7.** Effect of temperature on the photocatalytic degradation of quinoline. Conditions: flow rate = 0.35 L/min, pH = 6.7,  $C_0 = 40\text{ mg/L}$ , and the maximum irradiation intensity.



### 3.2.4. Effect of Aeration

Molecular oxygen is generally used as an electron acceptor to capture photo-generated electrons and form an active radical ( $O_2^-$ ). Therefore, quantum efficiencies may partly be increased by inhibiting electron-hole recombination to enhance the photocatalytic efficiency [25]. In the present study, compressed pure oxygen, pure nitrogen, and air were purged into the photocatalytic reactor to analyze the effect of dissolved oxygen on quinoline photodegradation. Figure 8 shows that the degradation percent of quinoline solution under pure oxygen aeration at the rate of 0.35 L/min reached 97% after continuous UV illumination for 60 min. This percentage was much higher than that under airflow or pure nitrogen aeration. Under pure nitrogen aeration, the percent quinoline degradation rapidly increased for the first 15 min, and then became constant with time. Therefore, molecular nitrogen clearly existed in air, and pure nitrogen aeration played a negative role in the photocatalytic reaction, playing a dual role. One was to reduce residual dissolved oxygen in water by continued stripping. The other was to relocate dissolved oxygen onto the  $TiO_2$  surface to inhibit the formation of active radicals, and retard the agitation effect to decrease the effective mass transfer for the photocatalytic process.

**Figure 8.** Effect of air, pure nitrogen, and pure oxygen aeration on the photodegradation of quinoline. Conditions: flow rate = 0.35 L/min, pH = 6.7,  $T = 17\text{ }^\circ\text{C}$ ,  $C_0 = 40\text{ mg/L}$ , and the maximum irradiation intensity.

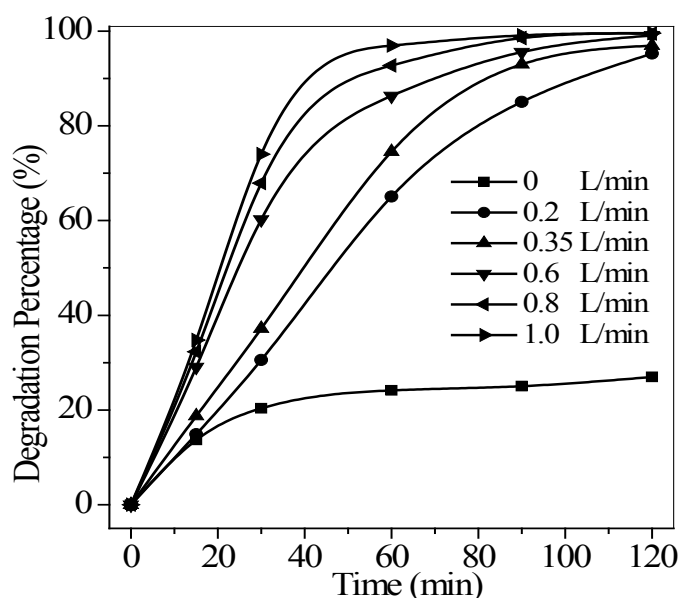


The relationship between airflow and degradation efficiency was also investigated, as shown in Figure 9. Percent quinoline degradation increased with increased air flow rate to 1.0 L/min, which suggested that higher air aeration rate favors to increase dissolving oxygen in water and agitate the solution to speed up mass transfer.

However, compared with pure nitrogen aeration, percent quinoline degradation under no airflow was still up to 20% after irradiation for 120 min, a little above 5% of that under pure nitrogen aeration at a rate of 0.35 L/min, as illustrated in Figure 8, although a similar increased removal tendency

presented in the initial stage because of the effect of residual dissolved oxygen. It's proposed that molecular oxygen was recycled in a single photocatalytic system such that reoxygenation equilibrium existed between oxygen consumption and steady-state replenishment. The reoxygenation processes may have also proceeded at low levels under no airflow, but were inhibited by pure nitrogen stripping.

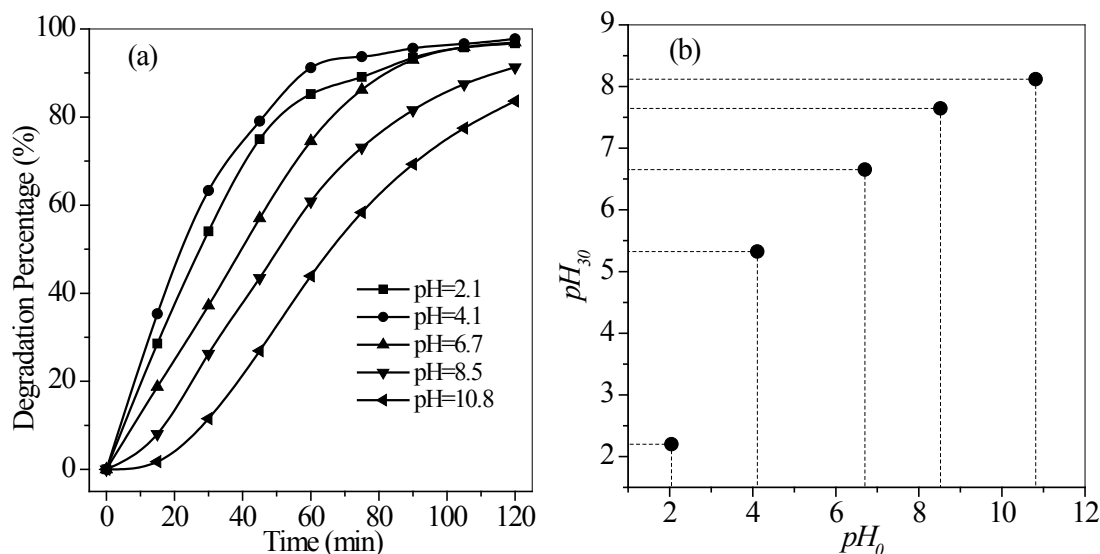
**Figure 9.** Effect of air flow on the photocatalytic degradation of quinoline. Conditions: pH = 6.7,  $T = 17\text{ }^{\circ}\text{C}$ ,  $C_0 = 40\text{ mg/L}$ , and the maximum irradiation intensity.



### 3.2.5. Effect of pH

The pH value of a solution determines the surface charge of photocatalysts and the ionization or speciation ( $pK_a$ ) of an organic pollutant [26,27]. Hence, pH varies significantly and can play an important role in the photocatalytic degradation of organic contaminants [28]. The effect of pH on quinoline degradation was investigated, as shown in Figure 10a. The degradation rate significantly increased at pH below 4.1, and then gradually decreased with increased pH from 6.7 to 10.8. An alkaline medium appeared to retard quinoline degradation, with the degradation percent below 10% during the first 15 min. A combined pH change analysis (Figure 10b) revealed that after UV irradiation for 30 min, the initial pH value of the solution shifted to the value of the point of zero charge ( $P_{zc}$ ) of  $\text{TiO}_2$  (Degussa P25), which is widely reported at pH 6.25 [29], *i.e.*, the initial pH increased from 4.1 to 5.3. These observed behaviors can be explained in terms of the  $P_{zc}$  of  $\text{TiO}_2$  and the  $pK_a$  (about pH 4.95) of quinoline [30]. At more alkaline pH values, the  $\text{TiO}_2$  surface is negatively charged. At pH values below 6.25, the surface is positively charged [31].

**Figure 10.** Effect of pH (a) on the photocatalytic degradation of quinoline and (b) after irradiation for 30 min. Conditions: flow rate = 0.35 L/min,  $T = 17\text{ }^{\circ}\text{C}$ ,  $C_0 = 40\text{ mg/L}$ , and the maximum irradiation intensity.  $\text{pH}_0$  and  $\text{pH}_{30}$  represent the pH values of the aqueous solution after UV irradiation for 0 and 30 min, respectively.



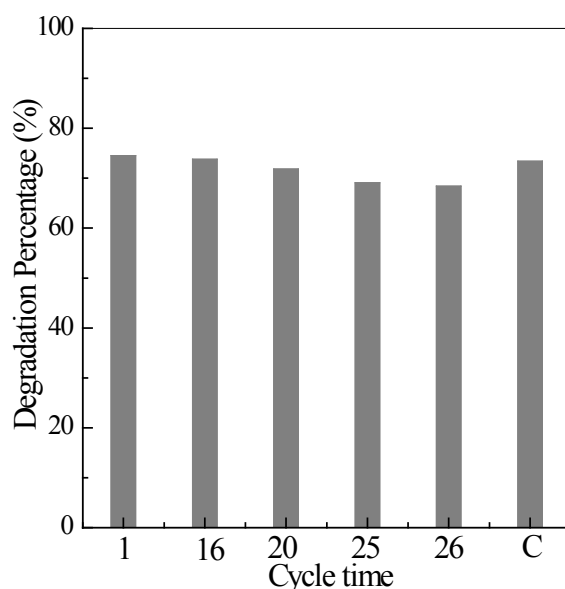
When the pH is above 6.25, the adsorption of quinoline molecules onto the  $\text{TiO}_2$  surface became difficult with increased pH due to the repellent effect of the two species with negative charges. However, within pH 4.95–6.25, the negatively charged quinoline molecules were easily adsorbed on the positively charged  $\text{TiO}_2$  surface. This phenomenon benefited the quinoline degradation. At pH values below the quinoline  $\text{pK}_a$  value, the quinoline molecules are present in the protonated form (with a positive charge), which did not favor the absorption onto the  $\text{TiO}_2$  surface, which also had a positive charge. The protonated form appeared to enhance the UV absorbance of quinoline, which led to the improvement in its degradation under acidic conditions compared with alkaline medium [32]. Also, at low pH values, a number of sulfur anions were found when the pH of the water was adjusted. These anions strongly hindered the generation of active radicals via competitive adsorption with  $\text{O}_2$ ,  $\text{H}_2\text{O}$ , and other molecules on the catalyst surface, resulting in decreased quinoline degradation in acidic medium. Therefore, the different pH values before and after the reaction for 30 min revealed that quinoline had a higher degradation rate at pH 4.95–6.25, whereas the degradation rate was moderately influenced by the solution pH.

### 3.2.6. Stability of the $\text{TiO}_2/\text{Ni}$ Film

The stability of the  $\text{TiO}_2/\text{Ni}$  film in the fabricated reactor is one of the most important factors for its practical application. Therefore, a recycling experiment was carried out using the same  $\text{TiO}_2/\text{Ni}$  film to investigate its stability. After each experiment, the  $\text{TiO}_2/\text{Ni}$  film was washed with distilled water for 30 min under air aeration, dried at  $105\text{ }^{\circ}\text{C}$  for 60 min in an electric oven, and then reused under one set of reaction conditions ( $[\text{quinoline}]_0 = 40\text{ mg/L}$ ,  $\text{pH} = 6.7$ , flow rate = 0.35 L/min, reaction temperature =  $17\text{ }^{\circ}\text{C}$ , and the maximum irradiation flux). An irradiation time of 60 min was selected for the recycling experiment due to the disappearance of the characteristic absorption of quinoline, as described in Figure 4. Figure 11 shows that the percent quinoline degradation remained constant

during the first 16 runs of photocatalytic reaction, obviously decreased in subsequent runs, and then declined to 70% after 25 runs. This finding was in accordance with the TiO<sub>2</sub>/Ni film varying in color from white to pale yellow. However, complete reactivation occurred after the TiO<sub>2</sub>/Ni film was subjected to calcinations. This reactivation was due to the decomposition of the adsorbed reactants at a high temperature.

**Figure 11.** Percent quinoline degradation of the TiO<sub>2</sub>/Ni film with consecutive runs under the conditions of  $T = 290$  K, flow rate = 0.35L/min, pH = 6.7,  $C_0 = 40$ mg/L, and the maximum irradiation flux. C denotes the re-calcinated TiO<sub>2</sub>/Ni film.

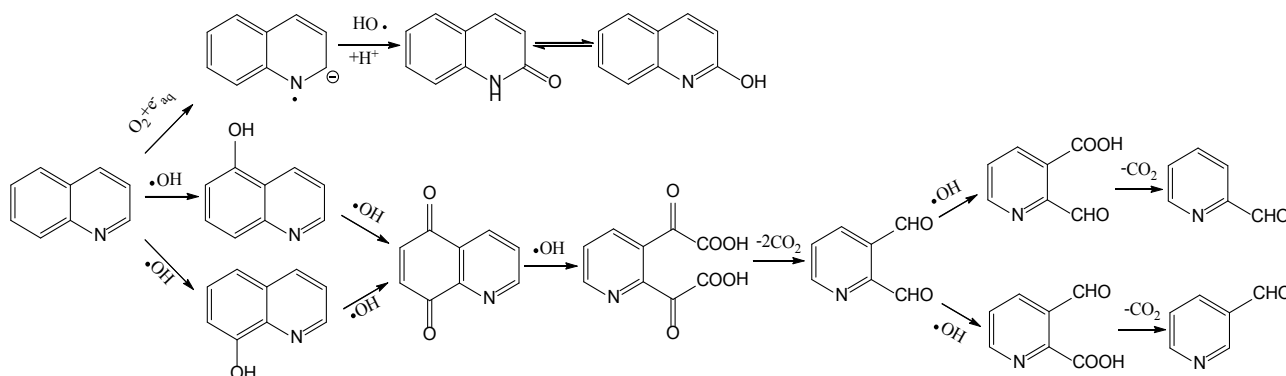


### 3.3. Mechanism of Quinoline Degradation

The synthetic wastewater containing quinoline varied in color, as described in Section 3.2, indicating that there existed some intermediate products in the photocatalytic process. Based on the GC/MS analysis performed, the effluent of the synthetic wastewater after irradiation for 30 min contained 2-pyridinecarboxaldehyde, 3-pyridinecarboxaldehyde, quinoline, and 2(1*H*)-quinolinone. Figure 12 shows the possible mechanisms for the formation of the three intermediate products. The formation of the first two intermediates may have depended on the electrophilic substitution between quinoline and hydroxyl radicals. The initial oxidation mainly occurred at positions 5 and 8 of the aromatic ring, resulting in the formation of 5,8-quinolinedione. Further oxidation by active radicals resulted in the formation of 2-pyridinecarboxaldehyde or 3-pyridinecarboxaldehyde based on the phenyl ring opening process via quinoline-5,8-dione. This mechanism was in accordance with that reported by Thomsen [33] and Zhu *et al.* [34]. Considering that the electron cloud density of the pyridine ring is lower than that of an aromatic ring, the pyridine ring is relatively difficult to be oxidized. Hence, the formation of 2(1*H*)-quinolinone is related to the superoxide ion ( $O_2^-$ ) generated by dissolved oxygen on the TiO<sub>2</sub> surface trapped electron under UV irradiation. Ishibashi *et al.* [35] have reported that the superoxide ion ( $O_2^-$ ) is generated at the water-TiO<sub>2</sub> interface with a longer lifetime of about 70 s. Its absolute number pre-illuminated is calculated to be  $2 \times 10^{14}/\text{cm}^2$ , and it has a low mobility [36]. During the adsorption of quinoline onto the TiO<sub>2</sub> surface, the initial addition

reaction between quinoline and the superoxide ion ( $O_2^-$ ) may take place at the C-2 position of the pyridine ring, similar with an ordinary nucleophile [34,37]. This phenomenon benefited the further reaction with active radicals to generate 2( $1H$ )-quinolinone.

**Figure 12.** Proposed pathways for the photocatalytic degradation of quinoline.



#### 4. Conclusions

A newly developed tubular photocatalytic reactor equipped with a  $TiO_2/Ni$  film was used for the photodegradation of an aqueous quinoline solution under different operational conditions. The results showed that percent quinoline removal increased with increased light intensity and air aeration. A lower photocatalytic degradation rate was shown under pure nitrogen aeration than under pure oxygen, air, or without any aeration. Percent quinoline removal decreased with increased total quinoline amount removal from 10 to 104.4 mg/L when the initial quinoline concentration was increased from 10 to 120 mg/L. The reaction temperature and pH should be at 30 °C and below 6.25, respectively, to obtain a high removal efficiency of quinoline from synthetic wastewater. The major intermediates of quinoline degradation were identified as 2-pyridinecarboxaldehyde, 3-pyridinecarboxaldehyde, and 2( $1H$ )-quinolinone. A primary degradation mechanism was proposed based on these intermediates. The new internal airlift loop tubular photocatalytic reactor based on a  $TiO_2/Ni$  film was proven to be very effective for quinoline removal from synthetic wastewater. The use of this reactor could hopefully be extended to treat other types of industrial wastewater.

#### Acknowledgements

The present research was sponsored by the Nature Science Foundation of China (50778036, 51108069 and 51008056), the PhD. Programs Foundation of the Ministry of Education of China (20100043110009), and the Social Development Foundation of Jilin Province (20060405, 20086035 and 201101002).

#### References

- Seo, J.S.; Keum, Y.S.; Li, Q.X. bacterial degradation of aromatic compounds. *Int. J. Environ. Res. Public Health* **2009**, *6*, 278-309.

2. Tao, X.Q.; Lu, G.N.; Liu, J.P.; Li, T.; Yang, L.N. Rapid Degradation of Phenanthrene by Using *Sphingomonas* sp. GY2B Immobilized in Calcium Alginate Gel Beads. *Int. J. Environ. Res. Public Health* **2009**, *6*, 2470-2480.
3. Kochany, J.; Maguire, R.J. Photodegradation of quinoline in water. *Chemosphere* **1994**, *28*, 1097-1110.
4. Alexei, N.; John, K. Parameters affecting the homogeneous and heterogeneous degradation of quinoline solutions in light-activated processes. *J. Photoch. Photobio. A* **1997**, *110*, 149-157.
5. Rockafellow, E.M.; Stewart, L.K.; Jenks, W.S. Is sulfur-doped TiO<sub>2</sub> an effective visible light photocatalyst for remediation? *Appl. Catal. B-Environ.* **2009**, *91*, 554-562.
6. Stewart, L.K. Tungsten Trioxide and Titanium Dioxide Photocatalytic Degradations of Quinoline. M.S. Thesis, Iowa State University, Ames, IA, USA, 2009.
7. Pichat, P. Photocatalytic degradation of aromatic and alicyclic pollutants in water: by-products, pathways and mechanisms. *Water. Sci. Technol.* **1997**, *35*, 73-78.
8. Kim, S.B.; Jang, H.T.; Hong, S.C. Photodegradation of gas-phase methanol and toluene using thin-film TiO<sub>2</sub> photocatalyst. 1. Influence of water vapor, molecular oxygen and temperature. *J. Ind. Eng. Chem.* **2002**, *8*, 156-161.
9. Xu, X.; Ji, F.Y.; Fan, Z.H.; He, L. Degradation of Glyphosate in Soil Photocatalyzed by Fe<sub>3</sub>O<sub>4</sub>/SiO<sub>2</sub>/TiO<sub>2</sub> under Solar Light. *Int. J. Environ. Res. Public Health* **2011**, *8*, 1258-1270.
10. Rodriguez, P.; Meille, V.; Pallier, S.; Al Sawah, M.A. Deposition and characterisation of TiO<sub>2</sub> coatings on various supports for structured (photo)catalytic reactors. *Appl. Catal. A-Gen.* **2009**, *360*, 154-162.
11. Yang, L.P.; Liu, Z.Y.; Shi, J.W.; Hu, H.; Shangguan, W.F. Design consideration of photocatalytic oxidation reactors using TiO<sub>2</sub>-coated foam nickels for degrading indoor gaseous formaldehyde. *Catal. Today* **2007**, *126*, 359-368.
12. Zhu, S.Y.; Yang, X.; Wang, G.N.; Zhang, L.L.; Zhu, H.F.; Huo, M.X. Facile Preparation of P25 Films Dip-Coated Nickel Foam and High Photocatalytic Activity for the Degradation of Quinoline and Industrial Wastewater. *Int. J. Chem. React. Eng.* **2011**, *9*, A37.
13. Taranto, J.; Frochot, D.; Pichat, P. Photocatalytic Treatment of Air: Comparison of Various TiO<sub>2</sub>, Coating Methods, and Supports Using Methanol or *n*-Octane as Test Pollutant. *Ind. Eng. Chem. Res.* **2009**, *48*, 6229-6236.
14. Olivier, R.; Muthukonda, V.S.; Maithaa K.D.; Loïc, S.; Nicolas, K.; Valérie, K. Solar light photocatalytic hydrogen production from water over Pt and Au/TiO<sub>2</sub> (anatase/rutile) photocatalysts: Influence of noble metal and porogen promotion. *J. Catal.* **2010**, *269*, 179-190.
15. Plantard, G.; Correia, F.; Goetz, V. Kinetic and efficiency of TiO<sub>2</sub>-coated on foam or tissue and TiO<sub>2</sub>-suspension in a photocatalytic reactor applied to the degradation of the 2,4-dichlorophenol. *J. Photoch. Photobio.* **2011**, *222*, 111-116.
16. Barakat, M.A. Adsorption and photodegradation of procion yellow H-EXL dye in textile wastewater over TiO<sub>2</sub> suspension. *J. Hydro-Environ. Res.* **2011**, *5*, 137-142.
17. Li, Y.M.; Gu, G.W.; Zhao, J.F.; Yu, H.Q.; Qiu, Y.L.; Peng, Y.Z. Treatment of coke-plant wastewater by biofilm systems for removal of organic compounds and nitrogen. *Chemosphere* **2003**, *52*, 997-1005.

18. Zhang, Y.H.; Yang, Y.N.; Xiao, P.; Zhang, X.N.; Lu, L.; Li, L. Preparation of Ni nanoparticle-TiO<sub>2</sub> nanotube composite by pulse electrodeposition. *Mater Lett.* **2009**, *63*, 2429-2431.
19. Bidault, F.; Brett, D.J.L.; Middleton, P.H.; Abson, N.; Brandon, N.P. A new application for nickel foam in alkaline fuel cells. *Int. J. Hydrogen. Energ.* **2009**, *34*, 6799-6808.
20. *JCPDS PDF-2 Release 2001*; ICDD: Newtown Square, PA, USA, 2001.
21. Kulovaara, M.; Corin, N.; Backlund, P.; Tervo, J. Impact of UV<sub>254</sub>-radiation on aquatic humic substances. *Chemosphere* **1996**, *33*, 783-790.
22. Bouanimba, N.; Zouaghi, R.; Laid, N.; Sehili, T. Factors influencing the photocatalytic decolorization of Bromophenol blue in aqueous solution with different types of TiO<sub>2</sub> as photocatalysts. *Desalination* **2011**, *275*, 224-230.
23. Qian, Ch.X.; Zhao, L.F.; Fu, D.F.; Li, L.; Wang, R.X. Study on the effect of temperature, humidity and light intensity on photocatalytic oxidation of NO<sub>2</sub> by Nano-TiO<sub>2</sub> immobilized on cement-based materials. *J. Environ. Sci. China* **2005**, *25*, 623-630.
24. Chen, D.W.; Ray, A.K. Photodegradation kinetics of 4-nitrophenol in TiO<sub>2</sub> suspension. *Water Res.* **1998**, *32*, 3223-3234.
25. Chung, H.H.; Mariñas, B.J. Role of Chlorine and Oxygen in the Photocatalytic Degradation of Trichloroethylene Vapor on TiO<sub>2</sub> Films. *Environ. Sci. Technol.* **1997**, *31*, 562-568.
26. Singh, H.K.; Saquib, M.; Haque, M.M.; Muneer, M. Heterogeneous photocatalyzed degradation of uracil and 5-bromouracil in aqueous suspensions of titanium dioxide. *J. Hazard. Mater.* **2007**, *142*, 425-430.
27. Singh, H.K.; Saquib, M.; Haque, M.M.; Muneer, M. Heterogeneous photocatalysed decolorization of two selected dye derivatives neutral red and toluidine blue in aqueous suspensions. *Chem. Eng. J.* **2008**, *136*, 77-81.
28. Lu, M.C.; Roam, G.D.; Chen, J.N.; Huang, C.P. Factors affecting the photocatalytic degradation of dichlorvos over titanium dioxide supported on glass, *J. Photochem. Photobiol. A.* **1993**, *76*, 103-110.
29. Renault, N.J.; Pichat, P.; Foissy, A.; Mercier, R. Study of the effect of deposited Pt particles on the surface charge of TiO<sub>2</sub> aqueous suspensions by potentiometry, electrophoresis and labeled ion adsorption. *J. Phys. Chem.* **1986**, *90*, 2733-2738.
30. Wang, S.L.; Zheng, Z.; Li, M. Pulse radiolysis mechanism study of quinoline in dilute solutions. *J. Radiat. Res. Proc. China* **2004**, *22*, 334-338.
31. Chen, D.W.; Ray, A.K. Photodegradation kinetics of 4-nitrophenol in TiO<sub>2</sub> suspension. *Water Res.* **1998**, *32*, 3223-3234.
32. Lapertot, M.; Pichat, P.; Parra, S.; Guillard, C.; Pulgarin, C. Photocatalytic degradation of p-halophenols in TiO<sub>2</sub> aqueous suspensions: halogen effect on removal rate, aromatic intermediates and toxicity variations. *J. Environ. Sci. Health A* **2006**, *41*, 1009-1025.
33. Thomsen, A.B. Degradation of quinoline by wet oxidation kinetic aspects and reaction mechanisms. *Water Res.* **1998**, *32*, 136-146.
34. Zhu, D.Z.; Sun, D.M.; Jiang, Z.L.; Wang, S.L.; Sun, X.Y.; Ni, Y.M. Studies on the Respective Reactions of Quinoline and Isoquinoline with Transient Species by Pulse Radiolysis. *Acta Phys. Chim. Sin.* **2008**, *24*, 2321-2326.

35. Ishibashi, K.I.; Fujishima, A.; Watanabe, T.; Hashimoto, K. Generation and Deactivation Processes of Superoxide Formed on TiO<sub>2</sub> Film Illuminated by Very Weak UV Light in Air or Water. *J. Phys. Chem. B* **2000**, *104*, 4934-4938.
36. Ishibashi, K.I.; Nosaka, Y.; Hashimoto, K.; Fujishima, A. Time-Dependent Behavior of Active Oxygen Species Formed on Photoirradiated TiO<sub>2</sub> Films in air. *J. Phys. Chem. B* **1998**, *102*, 2117-2120.
37. Wang, S.L.; Zhu, D.Z.; Sun, X.Y.; Shi, J.; Ni, Y.M.; Wang, W.F.; Yao, S.D. Spectral Analysis of Transient Species of Quinoline Degradation. *Spectrosc. Spect. Anal.* **2006**, *26*, 1479-1482.

© 2012 by the authors; licensee MDPI, Basel, Switzerland. This article is an open access article distributed under the terms and conditions of the Creative Commons Attribution license (<http://creativecommons.org/licenses/by/3.0/>).